Structure of the outer cusp and sources of the cusp precipitation during intervals of a horizontal IMF

Z. Němeček, J. Šafránková, L. Přech, J. Šimunek
Faculty of Mathematics and Physics, Charles University of Prague, Czech Republic

J.-A. Sauvaud, A. Fedorov, H. Stenuit
Centre d'Etude Spatiale des Rayonnements, CNRS, Toulouse, France

S. A. Fuselier
Lockheed Palo Alto Research Laboratory, Palo Alto, USA

S. Savin, L. Zelenyi
Institute of Space Research, Academy of Sciences, Moscow, Rusia

J. Berchem
University of California, Los Angeles, USA

Abstract. The cusp represents a place where the magnetosheath plasma can directly penetrate into the magnetosphere. Since the main transport processes are connected with merging of the interplanetary and magnetospheric field lines, the interplanetary magnetic field (IMF) orientation plays a decisive role in the formation of the high-altitude cusp. The importance of the sign of the IMF B_Z component for this process was suggested about 40 years ago and later it was documented by many experimental investigations. However, situations when IMF B_Z is the major IMF component are rather rare. The structure of the cusp during periods of a small IMF B_Z is generally unknown, probably due to the fully 3-D nature of the interaction. The present case study reveals the importance of horizontal IMF components on the global magnetospheric configuration as well as on small-scale processes at the cusp-magnetosheath interface. We have used simultaneous measurements of several spacecraft (ISTP program) operating in different regions of interplanetary space and two closely spaced satellites (INTERBALL-1/MAGION-4) crossing the cusp-magnetosheath boundary to show the connection between the short- and large-scale phenomena. In the northern hemisphere, observations suggest a presence of two spots of cusp-like precipitation supplied by reconnection occurring simultaneously in both hemispheres. A source of this bifurcation is the positive IMF B_Y component further enhanced by the field draping in the magnetosheath. This magnetic field component shifts the entry point far away from the local noon but in opposite sense in either hemisphere.

1. Introduction

The interaction of the interplanetary magnetic field (IMF) with Earth's magnetic field has a dominant effect on the magnetosphere as a mechanism for both plasma entry and for energy input from the solar wind. If reconnection occurs on the magnetopause, the mixture of magnetosheath and magnetospheric plasmas form a number of different boundary layers surrounding the magnetopause. An important question regarding reconnection is what determines its location on the magnetopause.

Paper number .
0148-0227/03/$9.00

1.1. Regions Associated With High-latitude Reconnection

For a given orientation of the magnetosheath magnetic field, it is not known how reconnection is distributed over the magnetopause. One possibility, referred to as "antiparallel merging", is that reconnection is favored to occur where the magnetosheath and magnetosphere fields are nearly antiparallel [*Crooker*, 1979]. Another possibility, referred to as "component merging", is that a shear in any component of the vector magnetic fields is sufficient for reconnection. In the case of a southward directed magnetosheath field, the subsolar magnetopause has been shown at times to be the preferred location for reconnection [*Gosling et al.*, 1990]. However, other studies have suggested that antiparallel merging may occur away from the subsolar region resulting in reconnection occurring at higher latitudes (e.g., [*White et al.*, 1998]). When the magnetosheath magnetic

field is directed northward, both antiparallel and component merging have been identified, but with differences in the magnetospheric interconnection. When antiparallel merging occurs, reconnection takes place poleward of the cusps. There is considerable observational evidence for this reconnection configuration coming from the low-altitude cusp measurements that exhibit a distinctive "reverse-dispersion" signature (e.g., [*Woch and Lundin*, 1992; *Matsuoka et al.*, 1996]), as well as from measurements at the high-latitude magnetopause [*Gosling et al.*, 1991; *Kessel et al.*, 1996]. Under northward magnetosheath field conditions, component merging may occur on the dayside magnetopause, equatorward of the cusp (e.g., [*Nishida*, 1989; *Onsager and Fuselier*, 1994; *Fuselier et al.*, 1995]). The connection would then be between the magnetosheath field and the closed dayside magnetospheric field lines. In these cases, reconnection may occur where the magnetic shear is relatively low.

An important consequence of high-latitude reconnection, that occurs poleward of the cusp for northward IMF, is the possible formation of an LLBL on closed field lines [*Song and Russell*, 1992; *Le and Russell*, 1996; *Lockwood and Moen*, 1999]. In this case, new closed magnetospheric field lines are formed by reconnection occurring in both the northern and southern hemispheres. The new closed field lines contain a mixture of magnetosheath and magnetospheric plasmas and may be transported downtail to contribute to the plasma sheet population. Alternatively, reconnected field lines can remain open for a long period of time on the dayside [*Fuselier et al.*, 1995].

The reconnection theory of the cusp predicts that the magnetosheath plasma will be seen within a layer on northward-pointing newly-opened field lines at the dayside magnetopause. This layer is referred as the "exterior" cusp or sometimes is called the "entry layer" or "front-side boundary layer (e.g., [*Haerendel et al.*, 1978]) or the (open) LLBL [*Paschmann et al.*, 1986]. The plasma in the exterior cusp is different from the magnetosheath proper. First, accelerated ions are present (but note that these are also found in the magnetosheath boundary layer formed by the open field lines outside the magnetopause [*Onsager et al.*, 2001]. Second, the plasma density is depressed because roughly one half of the sheath plasma is transmitted and the second half is reflected at the magnetopause [*Cowley*, 1982; *Fuselier et al.*, 1991]. Third, the ion velocity distributions are ordered by the magnetic field direction not by the magnetosheath flow. The cusp plasma is also observed on the southward-pointing field lines of the "interior" cusp along which the plasma precipitates into the ionosphere. It is also seen on the field lines that point anti-sunward/sunward with a small B_Z component in the northern/southern hemisphere, connecting the open LLBL with the magnetic cusp. Theory predicts that the ion precipitation can be continuously dispersed across the regions classified as (open) LLBL, cusp, mantle, and polar cap as the field lines evolve from the reconnection site into the tail lobe [*Lockwood*, 1997]. Most field lines will evolve anti-sunward close to the magnetic cusp. Spatial and temporal structures in reconnection mean that a continuous dispersion is not always be observed, but the fact that it is observed when reconnection is relatively steady and constant [*Onsager et al.*, 1993; *Lockwood et al.*, 1994] is highly significant.

Although many observational and theoretical investigations for southward and northward IMF have been presented, only a few observations dealt with the cases when IMF B_Y was dominant in the solar wind. *Fedorov et al.* [2001] have presented a case study of a flank magnetopause structure for an interval of duskward pointing (horizontal) IMF. These authors found that in a simple draped sheath field model, there is a large region where the magnetosheath field and IMF are antiparallel. In their case, the satellite (Interball-1) moved in the northern hemisphere and a steady state reconnection site was located at higher latitudes. Thus, the reconnection process started in a region sunward of the satellite. They found that in the presence of a strong flow shear, there is significant deviation from the simple 1-D de Hofman-Teller frame model. The authors attribute this deviation to the presence of sheared plasma flow.

Stenuit et al. [2001] have shown that the intensive but sporadic cleft-like precipitation can be found in extreme local times (6 or 18 MLT) and attributed it to low-latitude reconnection tailward of the cusp. The dawn - dusk occurrence rate was controlled by the IMF B_Y sign. The dispersion patterns were consistent with the time-of-flight effect.

1.2. High-altitude Cusp Locations

The high-altitude cusp occupies a broader region than can be expected from low- and middle-altitude observations (e.g., [*Aparicio et al.*, 1991; *Newell and Meng*, 1994; *Maynard et al.*, 1997]). This is true for the latitudinal as well as for the longitudinal extents of the high-altitude cusp. However, both the location of cusp precipitation and the direction of cusp-region plasma flow strongly depend on the orientation of the IMF and, maybe, on variations of the solar wind dynamic pressure. Based on $\sim$ 12000 cusp crossings provided by the Defense Meteorological Satellite Program (DMSP) in low altitudes, it has been shown that the cusp precipitation shifts: (1) equatorward during intervals of IMF $B_Z < 0$ nT [*Newell and Meng*, 1989]; (2) toward dawn for $B_Y < 0$ nT ($B_Y > 0$ nT) in the northern (southern) hemisphere [*Newell et al.*, 1989]; and (3) toward dusk for $B_Y > 0$ nT ($B_Y < 0$ nT) in the northern (southern) hemisphere. The B_Y shift is more apparent for $B_Z < 0$ nT than $B_Z > 0$ nT. The direction of cusp plasma flow is predominantly antisunward (sunward) for $B_Z < 0$ nT ($B_Z > 0$ nT) in the northern (southern) hemisphere [*Weiss et al.*, 1995]. During southward IMF, the cusp local magnetic time extent can reach 3.7 hours of MLT. This suggests that the merging process involves the whole dayside magnetopause [*Maynard et al.*, 1997].

At higher altitudes ($\sim 2\ R_E$), *Aparicio et al.* [1991] identified a magnetosheath type of particle precipitation in a well defined region with an average width of $\sim 2^o$ in invariant latitude. The population, which appeared to have its source in the cusp, was found in a region where the geomagnetic field lines were inferred to be closed; possibly 3^o-5^o equatorward of the region of open field lines [*Potemra et al.*, 1992]. Furthermore, they suppose that the solar wind/cusp plasma enters into closed geomagnetic field lines by a process associated with a time-varying magnetospheric configuration consisting of a compression and equatorward shift of the cusp, followed by a shift of the cusp to a position associated with northward IMF.

Woch and Lundin [1992] presented the magnetosheath plasma precipitation in the polar cusp and its control by IMF based on the Viking measurements. The azimuthal motion of accelerated magnetosheath plasma and the location of its entry in local time depends on IMF B_Y. Thus their

observation agrees with the observed shift of the cusp precipitation region toward dawn (dusk) for IMF B_Y negative (positive) as it was inferred in low-altitude measurements [*Newell et al.*, 1989]. The location in latitude (the equatorward or poleward boundary of the cusp) is controlled by IMF B_Z. For southward IMF, regions of accelerated plasma are located at the equatorward edge of the cusp, i.e., in the dayside merging region. For northward IMF, the acceleration site is at the poleward edge in agreement with the antiparallel merging hypothesis [*Crooker*, 1979].

Zhou et al. [2000] used the Polar magnetic and plasma measurements to determine the cusp position at radial distances between 5 and 9 R_E. Statistically, the cusp was located from 0800 to 1600 MLT ranges. The invariant latitude of the center of the cusp extended from 70° to 86° and moved further equatorward for stronger southward IMF. They observed a clear local time shift due to IMF B_Y only for southward IMF conditions. The observed local time shift (for $B_Z < 0$ nT) was again consistent with low-altitude observations [*Newell et al.*, 1989].

A statistical study of high-altitude cusp locations in the vicinity of the magnetopause by *Merka et al.* [2002] confirmed that when IMF B_Z becomes more negative, the cusp moves more equatorward (on $\sim 0.5°$ per 1 nT), but when IMF $B_Z > 0$ nT the cusp latitude is approximately constant. These MAGION-4 results on the cusp shift with IMF B_Z are consistent with the results obtained from DMSP at low altitudes [*Newell et al.*, 1989], Viking at middle altitudes [*Woch and Lundin*, 1992], and Polar and Hawkeye at high altitudes (e.g., [*Eastman et al.*, 2000; *Zhou et al.*, 2000]). At high-latitudes (82°–86° MLAT), *Merka et al.* [2002] observed an increased rate of the cusp-like plasma observation for northward IMF. Magnetosheath plasma enters these latitudes as a result of the reconnection process northward of the cusp as shown in *Safrankova et al.* [1998].

Merka et al. [2002] further demonstrated the influence of the IMF B_Y component on the high-altitude cusp position. The statistically documented dawnward (duskward) shift of the cusp location with increasing negative (positive) IMF B_Y in the northern hemisphere is consistent with the displacement of a possible high-latitude merging site. Moreover, the authors found the second peak of the cusp observation probability moving in the opposite sense and attributed this precipitation to reconnection in the southern hemisphere. A detailed analysis of the probability of the cusp encounter has shown that the observation of two sources of cusp precipitation, which was attributed to reconnection in conjugate hemispheres, is rather frequent. These two sources supply different MLT sectors and their separation seems to be controlled by IMF B_Y. The B_Y effect can explain the lower probability of cusp observations near the local noon: periods of negligible IMF B_Y are actually rare in the solar wind. The two cusp population can be separated in latitude probably during periods of negative B_Z and this fact influences the mean cusp positions. The possibility of the latitudinal separation of the two cusp sources were pointed out and then documented by the DMSP observations by *Wing et al.* [2001]. These authors presented an improved model of the entry of the solar wind plasma into the magnetosphere that incorporates the electric field obtained from statistical convection patterns. When IMF is strongly dusk/dawnward and weakly southward, their model predicts the occurrence of a double cusp near noon: one cusp at lower and one at higher latitudes. From their statistical results, it follows that the cusp latitudinal width increases and the equatorward boundary moves to lower latitudes with increasing IMF B_Y.

The brief overview given above leads to the conclusion that the IMF B_Y component would have a significant effect on the formation of high-latitude regions. Moreover, there is a clear understanding of a formation of magnetospheric regions when the IMF is directed southward and a little less clear understanding for northward pointing IMF. However, as it is documented by a statistics of the IMF direction presented in Figure 1, the IMF is more frequently horizontal, i.e., dominated by the B_X and/or B_Y components. The left part of the figure shows the distribution of the probability to observe a particular value of the IMF B_Z component. The statistics uses four years of nearly continuous monitoring of the IMF by WIND. As one can expect, the probability sharply peaks at $B_Z = 0$ and thus the other components frequently determine the IMF direction. The right part of the figure shows the probability distribution of the angle between the magnetic field and ecliptic plane. The figure demonstrates that for about 70% of time the declination of the IMF from the ecliptic plane is within ±30° and thus our study is relevant for a standard solar wind - magnetosphere interaction.

However, evidence of an IMF B_Y role reported so far are indirect - mainly statistical studies of precipitation patterns at low altitudes, modeling of the solar wind - magnetosphere interaction, etc. We have taken advantage of the ISTP era when many spacecraft were in a possible interaction region and/or were monitoring upstream and magnetospheric conditions in order to: (1) explain the influence of the horizontal IMF on the formation of the cusp region, (2) find the sources of the observed cusp precipitation, and (3) determine the global morphology of the high-latitude magnetosphere under such conditions.

Such study requires simultaneous measurements at many points in geospace and a good observational coverage of the cusp region in particular. As measurements of different points cannot be carried out exactly at the same time, a long period of stable upstream conditions and low geomagnetic activity has been selected for this study.

2. Observations

This study is based on the measurements made onboard seven ISTP spacecraft and two DMSP satellites. Their locations are shown in Figure 2 in GSM coordinates. The investigated time interval starts on February 18, 1997 at 23 UT and ends on February 19, 1997 at 03 UT. The locations of the distant spacecraft (IMP 8 located in the magnetosheath and GEOTAIL in the plasma sheet region) refer to 0000 UT on February 19, the coordinates of POLAR and INTERBALL-2 are given at 0200 UT. From Figure 2, one can note an excellent coverage of the northern high-latitude region. The morning sector of the high-altitude cusp was scanned by INTERBALL-1 and MAGION-4. At the same time, POLAR and INTERBALL-2 crossed the afternoon cusp sector at medium altitudes (POLAR: 55° – 78° INVLAT and 15 - 14 MLT from 0 to 3 UT, INTERBALL-2: 75° – 78° INVLAT and 18 - 12 MLT from 1 to 3 UT). The measurements were further supported by the observations of the DMSP-12 and 13 satellites in the auroral ionosphere.

2.1. Upstream Conditions and Geomagnetic Activity

Upstream conditions (solar wind parameters and IMF components) were monitored by WIND located at (209, 13,

-14)$_{GSM}$ R_E (we use the GSM coordinates throughout the paper). The proton number density was $n_{SW} \sim 9$ cm^{-3} and the velocity was $v_{SW} \sim 400$ km.s^{-1}. These values result in solar wind dynamic pressure fluctuating around $p_{SW} \sim 2.2$ nPa. The IMF was nearly horizontal, $B \sim (2.5, 2.5, 0)_{GSM}$ nT. The expected time of propagation of solar wind features from the WIND position to the INTERBALL-1/MAGION-4 location was ~ 55 minutes.

The IMF WIND measurements can be compared with IMP 8 data. IMP 8 was near the dusk magnetosheath at (-20, 34, -5)$_{GSM}$ R_E. The mean value of its magnetic field strength is similar to that as measured by WIND because IMP 8 was on the flank. A slightly different direction of $B_{IMP} \sim (2, 2, -2)$ nT can be attributed to the draping of the field lines against the magnetopause. Unfortunately, no IMP 8 plasma data are available for the period studied here.

The INTERBALL-1 data can be used for an estimation of magnetosheath conditions after 0155 UT when INTERBALL-1 entered the free-flow magnetosheath above the cusp. It observes the proton number density, $n_{MSH} \sim 15$ cm^{-3}, the velocity, $v_{MSH} \sim 230$ km.s^{-1}, and magnetic field, $B_{MSH} \sim (3, 12, -1)$ nT. These values of plasma density and magnetic field magnitude are consistent with the values measured upstream and mean compression of the magnetic field and plasma in the investigated region of the magnetosheath [*Nemecek et al.*, 2002].

The variations of upstream conditions during the interval under study are presented in Figure 3. The top panel shows the solar wind dynamic pressure. It is almost stable without significant jumps. The IMF magnitude and components in next two panels exhibit an exceptionally quiet behavior. IMF has an orthospiral orientation and it is probably the reason why the IMP 8 magnetic field components in the fourth and fifth panels exhibit large high-frequency fluctuations. However, mean values of the magnitude and components as well as the amplitude and frequency spectrum of fluctuations remain unchanged through the our time interval. The last two panels show the magnetic field as measured by GEOTAIL located in the plasma sheet. Again, the magnetic field is nearly constant, indicating a very low activity in the geomagnetic tail. Similarly, the data from geosynchronous satellites have been checked in order to search for changes connected with the magnetospheric activity. The plasma, particle fluxes, and magnetic field from GOES, LANL, etc. (not shown) show only standard changes caused by the Earth rotation.

The low level of geomagnetic activity is documented in Figure 4 where the D_{ST} and AE indexes are plotted. The D_{ST} is slightly negative and nearly constant, whereas the AE index exhibits a small increase at the end of the interval, but its magnitude still corresponds to a very low magnetic activity. Based on the examination of Figures 3 and 4, we can conclude that the investigated interval was quiet and provides a good opportunity for a multi-satellite study.

2.2. INTERBALL-1 and MAGION-4 Observations

The principal satellites for this study are INTERBALL-1 and MAGION-4, which were scanning the high-altitude cusp as displayed in Figure 5. The figure presents the Tsyganenko model field lines [*Tsyganenko and Stern*, 1996] computed using the WIND IMF and plasma data as an input. Plotted field lines cross the INTERBALL-1 location at 23, 0, 1, 2, and 3 UT (INTERBALL-1 moves upward and duskward). Thin black lines show the projection of the magnetic field vectors measured by INTERBALL-1 [*Klimov et al.*, 1997]. The shape of the model field lines suggests that INTERBALL-1 is located slightly poleward of the model cusp proper. Directions of the model and measured magnetic fields roughly coincide not only in the cusp but even after the black circle which marks the magnetopause crossing. It indicates a very low magnetic shear across the magnetopause ($\sim 20^o$).

An overview of INTERBALL-1 measurements is presented in Figure 6. As can be clearly seen, INTERBALL-1 crossed several regions whose boundaries are indicated by dashed vertical lines in the figure. From 2300 to 0050 UT, the antisunward ion flux (f_{VDP} in the first panel [*Safrankova et al.*, 1997]) is very low, indicating either stationary or tenuous plasma. A comparison of ion energy spectrograms [*Yermolaev et al.*, 1997] measured in antisunward (E_{C30}) and sunward (E_{C150}) directions (panels 6 and 7) shows that the plasma is indeed nearly at rest because the sunward energy flux is only a little higher than the tailward one. The flux peaks at an energy of ~ 300 eV. This region is identified as the cusp. This classification is confirmed by the magnitude and components of the magnetic field (2^{nd} and 3^{rd} panels). Note that until 0000 UT only spin averaged (2 min) data are available.

At 0050 UT, INTERBALL-1 entered a region with similar plasma characteristics, but with a highly fluctuating magnetic field. This region is usually called Turbulent Boundary Layer (TBL, e.g., [*Savin et al.*, 1997]) and represents an interface between the cusp proper and the magnetosheath. The outer boundary of the TBL, the magnetopause, was crossed at 0107 UT. As noted above, the magnetic shear across the magnetopause was low and thus the crossing cannot be reliably identified in the magnetic field data. However, a sharp increase of the ion flux displayed in the first panel as well as a clear change in ion energy spectrograms indicate that the satellite entered a region occupied by a dense plasma flowing in the tailward direction. The ion flux gradually increases until 0150 UT when the satellite reached the magnetosheath proper. Since the ion energy spectrograms do not change throughout this interval, we attribute the observed increase of the ion flux to the increase of the plasma density. This feature is clearly apparent in electron energy spectrogram (E_{e0} in the last panel [*Sauvaud et al.*, 1997]) and was confirmed by a computation of moments of 3-D ion distribution (not shown).

It is important to note that INTERBALL-1 can serve as a magnetosheath monitor after the magnetopause crossing. It provides the magnetosheath magnetic field which touches the magnetopause and thus allows us to determine a possible merging site with a better probability than can be done from the IMF measurements. Values of magnetic field components just after the magnetopause crossing were $B_{MSH} \sim (0, 12, 1)$ nT and this field remains nearly constant until the end of the interval. Such orientation suggests that antiparallel merging can occur duskward of the cusp in the northern hemisphere. Providing that the orientation of the magnetosheath magnetic field above the southern cusp is the same (the draping effect would be symmetric), we can expect antiparallel merging dawnward of the cusp in the southern hemisphere.

The boundary at 0150 UT is connected with a sharp change of the properties of the high-energy ion fluxes. These differential fluxes, measured by two differently oriented detectors, are shown in panels 4 and 5 of Figure 6. The

f_{DOKpar} panel displays the sunward particle fluxes with energies of about 50 and 100 keV, whereas the fluxes in the $f_{DOKperp}$ panel were measured by the detector rotating around the Sun-Earth line [*Kudela et al.*, 1995]. As the magnetosheath magnetic field was nearly perpendicular to this line, the $f_{DOKperp}$ detector records the fluxes parallel and antiparallel to the magnetic field in particular phases of a spacecraft spin. We will discuss the detailed behavior of these ions later. Note here that the ions are nearly isotropic until 0150 UT; however, they stream along the magnetic field after this time. Similar features can be seen simultaneously at lower energies in the ion spectrograms and even in the electron spectrogram (E_{e0}). These two populations of the high-energy ions are not divided by any magnetic signature.

The stability of the features observed by INTERBALL-1 is demonstrated by plasma and field measurements made onboard MAGION-4 (Figure 7) that crossed the same regions about 94 minutes later (as expected from the orbital delay). The behavior of the ion flux, f in the first panel, and magnetic field (2^{nd} and 3^{rd} panels) both in Figure 7 is very similar to that observed by INTERBALL-1 and thus one can identify the same boundaries. According to the ion energy spectrograms [*Nemecek et al.*, 1997], MAGION-4 was in the cusp until 0225 UT when the magnetopause was crossed. A comparison of the E_{I0} and E_{I180} spectrograms recorded in the tailward and sunward directions, respectively, shows nearly standing plasma with a small sunward velocity component. This plasma population is replaced by a tailward streaming magnetosheath-like population after the magnetopause crossing at 0225 UT. We can clearly see a gradual increase of the ion density in a layer just outside the magnetopause, between 0225 and 0245 UT. A similar layer registered by INTERBALL-1 was bounded by an abrupt change of the high-energy ion flow at its outer edge. Unfortunately, no high-energy particle measurements are available onboard MAGION-4 to be compared with INTERBALL-1 observations.

The E_{I90} spectrogram is from an analyzer rotating perpendicularly the Sun-Earth line. It exhibits high-count rate in the cusp where the speed of the plasma is low and its temperature high, and shows a strong spin modulation in the magnetosheath caused by the bulk speed of the plasma.

2.3. INTERBALL-2 Data

The ION instrument onboard INTERBALL-2 [*Sauvaud et al.*, 1998] was collecting plasma measurements on the dusk side of the auroral oval (from 1.8 to $3R_E$ of altitude) between 0000 UT and ~0142 UT when the communication with the satellite was stopped. From 0000 to 0032 UT, the satellite was located in the plasma sheet extension on the dayside (Figure 8). There, electrons have very low fluxes in the energy range $\sim 1-7$ keV, near the detection limit, while ion fluxes display characteristic energy variations: A gap in the flux is clearly seen with an upper energy cut-off decreasing from about 10 keV at 0000 UT (ILAT = 68.03°, MLT = 11.97 hours) down to $\sim$ 100 eV at 0038 UT. This is a common feature of the dayside plasma sheet due to the excessive drift time of the ions which could reach the gap [*Kovrazhkin et al.*, 1999]. The ions are lost by charge exchange with the neutral hydrogen of the geocoronna [*Stenuit*, 2002]. Note that ions with energies lower than $\sim$ 1 keV form the lower boundary of the gap. These ions are able to drift eastward from a nightside source under the effect of the corotating electric field [*Sauvaud et al.*, 1981]. Later on, INTERBALL-2 encounters an intense precipitation of electrons and a less intense precipitation of hydrogen ions, starting at latitudes of about 76°, accompanied with an outflow of low-energy oxygen ions between 0030 and 0100 UT.

INTERBALL-2 stays inside this region of the high low-energy fluxes until 0042 UT, when the telemetry was stopped. The highest latitude, 79.12°, was reached at 0100 UT at an MLT of 16.6 hours. A careful examination of the pitch-angle distributions shows that both electrons and H^+ ions exhibit a narrow loss-cone caused by the precipitation into the ionosphere, whereas the O^+ ions are streaming upward. These features indicate that INTERBALL-2 is probably located on open field lines after 0030 UT. A typical electron energy spectrum taken inside this region is displayed in Figure 9a (thick line) together with a magnetosheath energy spectrum taken onboard INTERBALL-1 at 0119:56 UT (dotted dashed line) and spectrum inside the outer cusp taken at 0010:02 UT (thin line). The electron spectra are quite similar in shape; however, the electron core temperature of the spectrum taken over the polar region is slightly higher than inside the outer cusp while fluxes are lower. Figure 9b displays the hydrogen energy spectrum taken onboard INTERBALL-2 and the ion spectrum taken inside the outer cusp onboard INTERBALL-1. While the spectra are also quite similar, a flux maximum around 2 kev is detected over the polar region which could indicate a plasma sheet population. We interpret the electron and ion structures as an indication of the spacecraft presence in the LLBL/cleft region.

2.4. POLAR Measurements

Figure 10 presents the ion data measured onboard POLAR by the TIMAS instrument [*Shelley et al.*, 1995] between 0000 and 0400 UT when the satellite sweeps across in the high-latitude post-noon sector at altitudes in a range $6.7-9\,R_E$. The ion gap is also clearly seen in the hydrogen spectrogram from 0000 UT until 0145 UT for latitudes ranging from 70° to 74.4°. Simultaneously, as for INTERBALL-2, drifting hydrogen (and oxygen) ions are detected at energies lower than those of the gap. Note the plasma sheet precipitation with energies in the range 10-20 keV at 0000 UT. Later, starting around 0150 UT, POLAR encounters a low-energy hydrogen precipitation, while plasma sheet ions are still being measured with the energy between 1 to 10 keV. As time progresses, the satellite moves towards higher latitudes. The energy of the plasma sheet precipitation slowly

Table 1. Parts of spacecraft orbits mapped in Figures 11 and 12.

Northern hemisphere		Southern hemisphere	
Satellite	Time interval	Satellite	Time interval
M4	23:00–4:00	DMSP12	21:00–21:21
IB1	23:00–2:30	DMSP12	22:45–23:00
IB2	0:00–2:00	DMSP12	0:25–0:40
Polar	1:00–4:00	DMSP12	2:07–2:22
DMSP12	22:02–22:12	DMSP12	3:52–4:07
DMSP12	23:42–23:51		
DMSP12	1:15–1:30		
DMSP12	2:58–3:11		
DMSP13	21:58–22:08		
DMSP13	23:35–23:50		
DMSP13	1:20–1:30		
DMSP13	2:58–3:13		

decreases, while the satellite is measuring several patches of low-energy ions. From these measurements, it can be concluded that POLAR is also encountering the LLBL/cleft.

2.5. Cusp/Cleft Location From Multispacecraft Observations

In order to compare the measurements of the available spacecraft, we have mapped their trajectories down to the DMSP height ($\sim$ 830 km) and plotted their footprints together with all DMSP passes in Figure 11 for the northern hemisphere. The mapped time intervals are given in Table 1 and roughly correspond to the intervals shown in the previous figures with the exception of INTERBALL-1 and MAGION-4, which are mapped only until the magnetopause crossing.

The marks on the spacecraft trajectories denote the locations where the cusp/cleft-like plasma was observed. We are not showing DMSP spectrograms for briefness, but the reader can find them on: sd-www.jhuapl.edu/Aurora/spectrogram/. Figure 11 shows that a cleft-type precipitation was observed in a broad range of local times (8 - 12.5 MLT) in the morning sector. The DMSP measurements are confirmed by the MAGION-4 and INTERBALL-1 observations which registered the cusp-like plasma along both projected trajectories shown in the figure. Although the coverage of the afternoon sector is not so good, we can make several important conclusions. First, none of the DMSP satellites saw the precipitation which could be classified as the cusp or cleft, but the precipitation observed by INTERBALL-2 and POLAR which map into the same region, exhibits the cleft features. However, the INTERBALL-2 ion number flux was significantly lower than usually observed in this region. It peaks around 10^6 particles/cm^2.s.sr.keV, whereas fluxes of the order 10^7 are frequently observed (e.g., [*Stenuit et al.*, 2001]). On the other hand, electron fluxes are comparable with the standard cusp/cleft precipitation at these altitudes. Thus the northern cusp/cleft region is shifted toward dawn from its average location.

A similar projection of the precipitation in the southern hemisphere is shown in Figure 12. Unfortunately, DMSP observations do not cover the dusk sector and thus we can only say that the cusp or cleft precipitation was observed in a broad range of morning local times, from 6 to 12 MLT.

3. Discussion of the Cusp Location

The observations presented in the previous section can be summarized as follows:

1. The upstream conditions were exceptionally stable and the geomagnetic activity was very low during the investigated interval. It gives us the possibility to compare measurements of the different spacecraft despite the fact that these observations were carried out at different times within the interval.

2. IMF was nearly horizontal in the solar wind (Figure 3, WIND observations) and, due to the draping effect, the positive IMF B_Y component was dominant above the northern cusp (Figure 6, INTERBALL-1 observations after 0140 UT).

3. INTERBALL-1, MAGION-4, DMSP 12, and DMSP 13 observed the cusp or cleft plasma between 8 and 12.5 MLT, i.e., in the morning sector of the northern auroral oval. None of the DMSP spacecraft crossing the afternoon sector observed patterns that could be classified as the cusp or cleft. A weak ion cleft-type precipitation was observed by INTERBALL-2 and POLAR at higher altitudes, only. It means that the cusp or cleft precipitations occupy nearly the entire dayside auroral oval. The maximum of the precipitation is shifted toward dawn from its average location.

4. DMSP 12 observed the cusp/cleft-like precipitation in the morning sector (6 - 12 MLT) of the southern auroral oval. We should point out that we do not distinguish the cusp and cleft precipitations for two reasons. First, these two regions (or plasma populations) cannot be reliably defined in high altitudes near the magnetopause [*Merka et al.*, 2000; 2002]. Second, both populations come from the same source (magnetosheath) and differ only slightly.

The magnetic field geometry which can explain the observations is schematically drawn in Figure 13. The thin black lines show the magnetopause magnetic field lines. IMF lines are shown in yellow, the places where they touch antiparallel magnetopause lines are distinguished by the green dots and corresponding magnetopause lines are blue. The position of INTERBALL-1 at the time of its magnetopause crossing is shown by the red dot. The sites favorable for antiparallel merging are located dawnward of the cusp in the southern hemisphere and duskward in the northern hemisphere. Based on the magnetic field locations and including earlier statistical findings [*Merka et al.*, 2002; *Newell et al.*, 1989], one would expect that the cusp or cleft precipitations would be observed in the afternoon (morning) sector of the northern (southern) auroral oval and vice versa. However, Figures 11 and 12 show that it is true in the southern hemisphere but more intensive cusp/cleft-like precipitation was observed in the morning part of the northern auroral oval.

We suggest that the source of the cusp-like plasma observed in the dawn sector of the northern hemisphere is reconnection in the southern hemisphere. The field line reconnected there has two parts. One of them is connected to the southern, whereas the second to the northern cusp, both in corresponding dawn sectors. The magnetosheath plasma proceeds in both directions along the reconnected field line. However, the distance from a reconnection site to the observational point in the conjugated hemisphere is rather long, the particle distribution underwent an evolution and thus the precipitation patterns in the northern hemisphere were classified as the LLBL (cleft) in the DMSP data. This suggestion is partly consistent with the statistical findings of *Merka et al.* [2002] that during intervals of significant IMF B_Y, the probability of the cusp/cleft observations shows two maxima: one at dawn and the other at dusk sector. These two maxima were attributed to reconnection in the opposite hemispheres. We assume that a weak ion precipitation observed by INTERBALL-2 and POLAR together with a more intense electron precipitation observed by INTERBALL-2 at the dusk sector originate at the northern reconnection site. On the other hand, the DMSP measurements at the southern dawn auroral zone were classified as the cleft and even as the cusp near the local noon.

We suppose that this north-south asymmetry is connected with the tilt of the Earth's dipole. The northern hemisphere was tilted away from the Sun, the tilt angle ranged from -12^o to -20^o during the studied interval and thus a magnetosheath speed at the northern reconnection site was highly supersonic ($M_A \sim 2.3$ according to the INTERBALL-1 data). There is no magnetosheath monitor above the southern cusp, but we know that this cusp

is tilted toward the Sun, and thus, according to the gas-dynamic model of the magnetosheath flow [*Spreiter et al.*, 1966], it would be in the region of subsonic flow. The subsonic velocity together with the antiparallel fields result in an intensive reconnection dawnward of the southern cusp. This reconnection then supplies precipitation observed by the DMSP spacecraft in both hemispheres. The problem of the northern reconnection site will be discussed in the next section.

4. Reconnection Layer

The plasma parameters derived from ion energy spectrograms are plotted in Figure 14 together with the magnetic field magnitude and calculated Alfvén velocity, v_A. The magnetopause crossing (dashed vertical line) coincides with transition of the subsonic flow regime to supersonic one. However, the reconnection process under a strong flow shear is still not well understood. As we have suggested above, the supersonic flow prevents the cusp precipitation from a possible antiparallel merging site. The question is whether reconnection is inhibited or whether reconnection occurs, but cannot supply the ion precipitation. We suggest that this problem can be solved by an analysis of the high-energy particle fluxes. Figure 15 shows 2-D cuts of 3-D ion velocity distributions in flow-field-aligned magnetosheath coordinates. The vertical axis of the cut is aligned with the magnetosheath magnetic field and the plane contains the magnetosheath velocity vector. We would like to point out that the magnetosheath magnetic field is roughly oriented in the $+Y$ direction, whereas the velocity, $v_{MSH} \sim (-170, 0, 150)$ km.s^{-1} is nearly perpendicular to this magnetic field, and thus the horizontal axis of the cuts represents the velocity direction. The first panel in Figure 15 presents the body of the ion distribution inside the layer of gradually increasing ion flux (Figure 6). INTERBALL-1 observed there a typical magnetosheath distribution. The second panel shows the same distribution in a different color scale in order to distinguish the high-energy part of the distribution. This part is nearly symmetric with a lack of particles streaming along the magnetic field. However, the sensitivity of the plasma spectrometer providing 3-D distributions is marginally sufficient and the energy range is limited to 30 keV, and thus we will complement this analysis using the data of the DOK high-energy particle detector.

Figure 16 (a,b,c parts) presents differential ion fluxes for three energies ($E = 23, 51, 111$ keV) together with the corresponding pitch angles in the cusp proper (Figure 16a), in the layer of gradually increased density (Figure 16b), and in the magnetosheath proper (Figure 16c). In the cusp proper (0044-0050 UT), DOK observed fluctuating flux of all three energies. As fluctuations are not correlated with the detector pitch angle, we can deduce that the ion population of the selected energies is roughly isotropic. During the next time interval, from 0110 to 0116 UT, the fluxes for the two lower energies exhibit clear dropouts at pitch angles from ~ 0 to 60°. The hardness of the energy spectrum being approximately the same as that in the previous figure, we can conclude that the particles in both regions come from the same source. As shown in Figure 16c, the fluxes in the magnetosheath proper (0152-0158 UT) are significantly different. Ions of the lowest energy, 23 keV, are simply streaming antiparallel to the magnetic field, as significant fluxes were recorded only for pitch angles above 90°. The 51 keV ions exhibit a trapped distribution with the peaks around 90°. If we suppose that the particles are coming from a restricted region of the bow shock, these observations can be simply explained by the combined effects of the particle parallel velocity and of the $\mathbf{E} \times \mathbf{B}$ drift velocity inside the magnetosheath. Connection exists between the satellite and the acceleration region for the particles of low energy and small pitch angles as well as for the particles of high energy and larger pitch angles that the parallel velocity and the $\mathbf{E} \times \mathbf{B}$ drift length are roughly the same for all particles. However, the distributions of 51 and 111 keV protons in Figure 16c are not gyrotropic. This behavior can be more distinctly seen in the flux of 111 keV ions where particles are detected only during one half of the spacecraft spin. These features are typical for particles near an absorbing boundary (e.g., [*Oksavik et al.*, 2002]. A comparison of fluxes at different energies shows that the spectrum is much harder than that in the previous time intervals and thus we can expect a different source for these particles.

A possible explanation of these observations is schematically depicted in Figure 17. The magnetosheath field lines (line A in the figure) contain high-energy particles streaming from the dusk bow shock (note that the dusk bow shock was quasiparallel under the actual IMF orientation). If the distance of the magnetosheath field line to the magnetopause becomes smaller than two gyroradii for some energy, the corresponding ions are lost after the magnetopause crossing and the pitch-angle distribution would look like that in Figure 6c (line B in Figure 17). Nearer to the Earth at the location C, we encounter the reconnected field line. This line is disconnected from the dusk bow shock and is populated by high-energy particles from the cusp. It means that this line contains the magnetosheath plasma and the high-energy particles leaking from the cusp. We can conclude that the layer of gradually increased density observed by INTERBALL-1 between 0107 and 0150 UT and by MAGION-4 between 0224 and 0240 UT is the layer of newly reconnected field lines. This layer would be bounded by a slow shock [*Petschek*, 1995] and indeed, we can identify a ion flux enhancement complemented with magnetic field depletion at the outer edge of this layer (Figure 6). The kinks created on the field line after reconnection are pulled tailward by the magnetosheath flow and dawnward/duskward by the magnetic tension. However, as the magnetosheath flow is super-alfvenic, the tailward motion dominates and thus the plasma acceleration during reconnection is not able to turn the plasma into the cusp and to supply precipitation inside the cusp.

The reconnection layer seems to be very thick because it is observed by INTERBALL-1 for $\sim$ 43 minutes. However, a thickness of the layer cannot be determined from a satellite speed, only. The exact magnetopause geometry and, consequently, the angle between the magnetopause and INTERBALL-1 trajectory is unknown. Measurements of high-energy particles suggest that the satellite moved rather along the magnetopause than perpendicularly to it. The pitch-angle distribution like that in Figure 16c was observed for $\sim$ 40 minutes and such distribution can be observed only up to two gyroradii from the magnetopause. As the gyroradius of 111 keV protons was $\sim$ 3500 km, the thickness of the reconnection layer was about $\sim$ 6000 km in the discussed case. This is consistent with the estimations based on two-point measurements given, for example, in *Safrankova et al.* [1998].

5. Implications for a Global Magnetospheric Morphology

Reconnection of interplanetary and magnetospheric magnetic field lines is controlled by the magnetic shear at the magnetopause, i.e., by the direction of the magnetosheath magnetic field above the magnetopause. If this field has dominating $+B_Y$ component, the reconnection sites are located dawnward of the southern cusp and duskward of the northern cusp as shown in Figure 18. This figure is basically the same as Figure 13 illustrating the source of the cusp precipitation. However, we have added field lines reconnected in the northern hemisphere because we suppose that observations of high-energy particles are consistent with this reconnection. In the northern hemisphere, one part of the reconnected field line is pushed by magnetic tension across the high-latitude magnetosheath and becomes the mantle magnetic field line. The kink on the other part of the line moves with the Alfvén velocity, v_A duskward and southward and it is convected tailward with a magnetosheath velocity, v_{MSH} (Figure 18). In our case, $v_{MSH} \gg v_A$ above the reconnection site but reconnection can add only $\sim v_A$ to the magnetosheath plasma. Thus the bulk of ions would move generally tailward and only a small part of the ions could be directed toward the ionosphere. On the other hand, the magnetosheath speed is much smaller than the electron thermal speed and thus the behavior of the electrons is influenced only a little by the supersonic speed above cusp. We suppose that this fact can explain why INTERBALL-2 observed different ion and electron precipitation patterns.

The reconnected line (Figure 18) crosses the low-latitude region and thus such lines create the open LLBL on the dusk flank. The dawn LLBL is created by reconnection in the southern hemisphere. The aforementioned effects contribute to the tail twisting already expected as a result of the IMF B_Y component [*Nishida*, 1989]. The LLBL lines are populated with a mixture of the magnetosheath plasma and reconnection products. This reconnection can be intermittent due to the fluctuations of the magnetosheath magnetic field and thus the observer would encounter blobs of injected plasma. In the present case, the dusk LLBL would contain a significant portion of the high-energy particles from the bow shock region, whereas the dawn LLBL would not.

6. Conclusion

We have presented an extensive multipoint study of the cusp/LLBL regions during a prolonged interval of stable horizontal IMF. Our case study has shown that:

- Magnetopause reconnection can proceed in the regions of supersonic magnetosheath flow above the winter cusp.
- Such reconnection cannot supply the cusp-type precipitation. If observed, the precipitation patterns are classified as the LLBL/cleft.
- The cusp/cleft precipitation can be supplied by reconnection occurring in the conjugated hemisphere.
- The reconnection sites at both hemispheres are projected onto different local time sectors of the auroral oval during intervals of a significant IMF B_Y component. The magnetosheath velocity at the reconnection site is then a principal factor determining which of them exhibit cusp/cleft characteristics.
- Reconnection dawnward/duskward of the cusp caused by the IMF B_Y component is a source of the tail twisting.

We should point out that the above conclusions are based on a comprehensive study of one event. This event exhibited standard upstream conditions and thus we assume that the principles have a general applicability.

Acknowledgments. We thank K. W. Ogilvie and R. P. Lepping for providing the IMF and plasma data. The study was iniciated at the ISSI workshop on "Multi-scale dynamic processes in the magnetospheric boundary layers and cusp". The authors from Charles University acknowledge the support of Research Project, MSM 113200004 and the Czech Grant Agency, Contract 205/02/0947, and partly by the Charles University Grant Agency, Contract 191/02. Research at Lockheed Martin was supported by the NASA Polar Data Analysis Contract.

References

Aparicio, B., B. Thelin, and R. Lundin, The polar cusp from a particle point of view: A statistical study based on Viking data, *J. Geophys. Res.*, *96*(A8), 14023–14031, 1991.

Cowley, S. W. H., The causes of convection in the Earth's magnetosphere: A review of developments during the IMS, *Rev. Geophys.*, 20,531, 1982.

Crooker, N. U., Dayside merging and cusp geometry, *J. Geophys. Res.*, *84*, 951–959, 1979.

Eastman, T. E., S. A. Boardsen, S.-H. Chen, S. F. Fung, and R. L. Kessel, Configuration of high-latitude and high-altitude boundary layers, *J. Geophys. Res.*, *105*, 23221, 2000.

Fedorov, A., E. Dubinin, P. Song, A. Skalsky, and E. Budnik, Structure of the flank magnetopause for horizontal IMF: Interball-1 observations, *J. Geophys. Res.*, *106*, 25,419–25,436, 2001.

Fuselier, S. A., B. J. Anderson, and T. G. Onsager, Particle signature of magnetic topology at the magnetopause: AMPTE/CCE observations, *J. Geophys. Res.*, *100*, 11,805, 1995.

Fuselier, S. A., K. J. Trattner, and S. M. Petrinec, Cusp observations of high- and low-latitude reconnection for northward IMF, *J. Geophys. Res.*, *105*, 253, 2000.

Fuselier, S. A., S. M. Petrinec, and K. J. Trattner, Stability of the high-latitude reconnection site for steady northward IMF, *Geophys. Res. Lett.*, *27*, 473, 2000.

Gosling, J. T., M. F. Thomsen, S. J. Bame, R. C. Elphic, and C. T. Russell, Plasma tlow reversals at the dayside magnetopause and the origin of asymmetric polar cap convection, *J. Geophys. Res.*, *95*, 8073, 1990.

Gosling, J. T., M. F. Thomsen, S. J. Bame, R. C. Elphic, and C. T. Russell, Observations of reconnection of interplanetary and lobe magnetic field lines at the high-latitude magnetopause, *J. Geophys. Res.*, *96*, 14,097, 1991.

Haerendel, G., G. Paschmann, N. Sckopke, H. Rosenbauer, and P. C. Hedgecock, The frontside boundary layer of the magnetosphere and the problem of reconnection, *J. Geophys. Res.*, *83*, 3195, 1978.

Kessel R. L., S.-H. Chen, J. L. Green, S. F. Fung, S. A. Boardsen, L. C. Tan, T. E. Eastman, J. D. Craven, and L. A. Frank, Evidence of high-latitude reconnection during northward IMF: Hawkeye observations, *Geophys. Res. Lett.*, *23*, 583, 1996.

Klimov, S., et al., ASPI experiment: Measurements of fields and waves onboard the Interball-1 spacecraft, *Ann. Geophys.*, *15*, 514–527, 1997.

Kovrazhkin, R. A., J.-A. Sauvaud, and D. C. Delcourt, Interball-Auroral observations of 0.1-12 keV ion gaps in the diffuse auroral zone, *Ann. Geophys.*, *17*, 734, 1999.

Kudela, K., M. Slivka, J. Rojko, and V. N. Lutsenko, The apparatus DOK-2 (project INTERBALL): Output data structure and modes of operation, *Tech. Rep. UEF-01-95*, pp.65, Institute of Experimental Physics, Slovak Academy of Science, Kosice, Slovakia, 1995.

Le, G., and C. T. Russell, ISEE observations of low-latitude boundary layer for northward interplanetary magnetic field: Implications for cusp reconnection, *J. Geophys. Res.*, *101*, 27,239, 1996.

Lockwood, M., T. G. Onsager, C. J. Davis, M. F. Smith, and W. F. Denig, The characteristics of the magnetopause reconnection X-line deduced from low-altitude satellite observations of cusp ions, *Geophys. Res. Lett.*, *21*, 2757, 1994.

Lockwood, M., Energy and pitch-angle dispersions of LLBL/cusp ions seen at middle altitudes: Predictions by the open magnetosphere model, *Ann. Geophys.*, *15*, 1501, 1997.

Lockwood, M., and J. Moen, Reconfiguration and closure of lobe flux by reconnection during northward IMF: Evidence for signatures in cusp/cleft auroral emissions, *Ann. Geophys.*, *17*, 996, 1999.

Matsuoka, A., K. Tsuruda, H. Hayakawa, T. Mukai, and A. Nishida, Electric field structure and ion precipitation in the polar region associated with northward interplanetary magnetic field, *J. Geophys. Res.*, *101*, 10,711, 1996.

Maynard, N. C., E. J. Weber, D. R. Weimer, J. Moen, T. Onsager, R. A. Heelis, and A. Egeland, How wide in magnetic local time is the cusp? An event study, *J. Geophys. Res.*, *102*(A3), 4765–4776, 1997.

Měrka, J., J. Šafránková, Z. Němeček, S. Savin, and A. Skalsky, High-altitude cusp: INTERBALL observations, *Adv. Space Res.*, *25*, No. 7–8, 1425–1434, 2000.

Měrka, J., J. Šafránková, and Z. Němeček, Cusp–like plasma in high altitudes: A statistical study of the width and location of the cusp from MAGION-4, *Annales Geophysicae*, *20*, 311–320, 2002.

Němeček, Z., A. Fedorov, J. Šafránková, and G. Zastenker, Structure of the low-latitude magnetopause: MAGION-4 observations, *Ann. Geophys.*, *15*, 553–561, 1997.

Němeček, Z., M. Hayosh, J. Šafránková, G. N. Zastenker, and J. D. Richardson, The dawn-dusk asymmetry of the magnetosheath: Interball-1 observations, *Adv. Space res.*, in print.

Newell, P. T. and C.-I. Meng, Dipole tilt angle effects on the latitude of the cusp and cleft/low-latitude boundary layer, *J. Geophys. Res.*, *94*(A6), 6949–6953, 1989.

Newell, P. T. and C.-I. Meng, Ionospheric projections of magnetospheric regions under low and high solar wind pressure conditions, *J. Geophys. Res.*, *99*, 273–286, 1994.

Newell, P. T., C.-I. Meng, D. G. Sibeck, and R. P. Lepping, Some low-altitude cusp dependencies on the interplanetary magnetic field, *J. Geophys. Res.*, *94*(A7), 8921–8927, 1989.

Nishida, A. Can random reconnection on the magnetopause produce the low-latitude boundary layer?, *Geophys. Res. Lett.*, *16*, 227, 1989.

Oksavik, K., T. A. Fritz, Q.-G. Zong, F. Soraas, B. Wilkinen, Three-dimensional energetic ion sounding of the magnetopause using Cluster/RAPID, *Geophys. Res. Lett.*, in print.

Onsager, T. G., C. A. Kletzing, J. B. Austin, and H. MacKiernan, Model of magnetosheath plasma in the magnetosphere: Cusp and mantle particles at low altitudes, *Geophys. Res. Lett.*, *20*, 479, 1993.

Onsager, T. G., and S. A. Fuselier, The location of magnetopause reconnection for northward and southward interplanetary magnetic field, in *Solar System Plasmas in Space and Time*, *Geophys. Monogr. Ser.*, vol. 84, edited by J. L. Burch and J. H. Waite, p. 183, AGU, Washington, D. C., 1994.

Onsager, T. G., J. D. Scudder, M. Lockwood, and C. T. Russell, Reconnection at the high-latitude magnetopause during northward magnetic field conditions, *J. Geophys. Res.*, *106*, 25,467–25,488, 2001.

Paschmann, G., I. Papamastorakis, W. Baumjohann, N. Scopcke, C. V. Carlson, et al., The magnetopause for large magnetic shear; AMPTE/IRM observations, *J. Geophys. Res.*, *91*, 11,099–11,115, 1986.

Petschek, H. E., The concept of rapid magnetic field reconnection: A retrospection view, in *Physics of the magnetopause*, Gephys. Monogr. Ser., vol. 90, edited by P. Song, B. U. O. Sonnerup, and M. F. Thomsen, pp.21–28, AGU, Washington, D. C., 1995.

Potemra, T. A., R. E. Erlandson, L. J. Zanetti, R. L. Arnoldy, J. Woch, and E. Friis-Christensen, The dynamic cusp, *J. Geophys. Res.*, *97*(A3), 2835–2844, 1992.

Šafránková, J., G. Zastenker, Z. Němeček, A. Fedorov, M. Simerský, and L. Přech, Small scale observation of the magnetopause motion: Preliminary results of the INTERBALL project, *Annales Geophysicae*, *15*, 562, 1997.

Šafránková, J., Z. Němeček, D. G. Sibeck, L. Přech, J. Měrka, and O. Santolík, Two-point observation of high-latitude reconnection, *Geophys. Res. Lett.*, *25*, 4301–4304, 1998.

Sauvaud, J.-A., J. Crasnier, K. Mouala, R. A. Kovrazhkin, and N. V. Jorjio, Morning sector ion precipitation following substorm injections, *J. Geophys. Res.*, *86*, 3430, 1981.

Sauvaud, J.-A., P. Koperski, T. Beutier, H. Barthe, C. Aoustin, J. J. Throcaven, J. Rouzaud, E. Penou, O. Vaisberg, and N. Borodkova, The INTERBALL- Tail ELECTRON experiment: Initial results on the low-latitude boundary layer of the dawn magnetosphere, *Ann. Geophys.*, *15*, 587–595, 1997.

Sauvaud, J.-A., H. Barthe, C. Aoustin, J. J. Thocaven, J. Rouzaud, E. Penou, R. A. Kovrazhkin, and K. G. Afanasiev, The ION experiment onboard INTERBALL-Auroral satellite: Initial results on velocity dispersed structures in the cleft and inside the auroral oval, *Ann. Geophys.*, *16*, 1056, 1998.

Savin, S. P. et al., Interball tail probe measurements in outer cusp and boundary layers, in *Geospace Mass and Energy Flow: Results from the International Solar-Terrestrial Physics Program*, edited by J. L. Horwitz, D. L. Galagher and W. K. Peterson, Geophysical Monograph 104, American Geophysical Union, Washington D.C., 25–44, 1998.

Shelley, E. G., et al., The toroidal imaging mass-angle spectrograph (TIMAS) for the Polar mission, *Space Sci. Rev.*, *71*, 497, 1995.

Song, P., and C. T. Russell, Model of the formation of the low-latitude boundary layer for strongly northward interplanetary magnetic field, *J. Geophys. Res.*, *97*, 1411, 1992.

Spreiter, J. R., A. L. Summers, and A. Y. Alksne, Hydromagnetic flow around the magnetosphere, *Planet. Space Sci.*, *14*, 223, 1966.

Stenuit, H., Etude de la source solaire et des pertes de plasma de la magnetosphere terrestre a l'aide des satellites Interball, PhD thesis, University of Toulouse, January 2002.

Stenuit, H., J.-A. Sauvaud, D. C. Delcourt, T. Mukai, S. Kokubun, M. Fujimoto, N. Y. Buzulukova, R. A. Kovrazhkin, R. P. Lin, and R. P. Lepping, A study of ion injections at the dawn and dusk polar edges of the auroral oval, *J. Geophys. Res.*, *106*, 29,619–29,631, 2001.

Tsyganenko, N. A., and D. P. Stern, A new-generation global magnetosphere field model based on spacecraft magnetometer data, *ISTP Newsletter*, 6/1, 21, 1996.

Weiss, L. A., P. H. Reiff, E. J. Weber, H. C. Carlson, M. Lockwood, and W. K. Peterson, Flow-aligned jets in the magnetoshperic cusp: Results from the Geospace Environment Modeling Pilot program, *J. Geophys. Res.*, *100*(A5), 7649–7659, 1995.

White, W. W., G. L. Siscoe, G. M. Erickson, Z. Kaymaz, N. C. Maynard, K. D. Siebert, B. U. O. Sonnerup, and D. R. Weimer, The magnetospheric sash and the cross-tail S, *Geophys. Res. Lett.*, *25*, 1605, 1998.

Williams, D. J., Magnetopause characteristic inferred from three-dimensional energetic particle distribution, *J. Geophys. Res.*, *84*, 6385, 1979.

Wing, S., P. T. Newell, and J. M. Ruohoniemi, Double cusp: Model prediction and observational verification, *J. Geophys. Res.*, *106*, 25,571–25,593, 2001.

Woch, J., and R. Lundin, Signatures of transient boundary layer processes observed with Viking, *J. Geophys. Res.*, *97*(A2), 1431–1447, 1992.

Yermolaev, Y. I., A. O. Fedorov, O. L. Vaisberg, V. M. Balebanov, Y. A. Obod, R. Jimenez, J. Fleites, L. Liera, and A. N. Omelchenko, Ion distribution dynamics near the Earth's bow shock: First measurements with the 2-D ion energy spectrometer CORALL on the INTERBALL/Tail-probe satellite, *Ann. Geophys.*, *15*, 533, 1997.

Zhou, X. W., C. T. Russell, and G. Le, Solar wind control of the polar cusp at high altitude, *J. Geophys. Res.*, *105*, 245–251, 2000.

Z. Němeček, J. Šafránková, L. Přech, J. Šimunek, Faculty of Mathematics and Physics, Charles University of Prague, V Holesovickach 2, 180 00 Praha 8, Czech Republic. (zdenek.nemecek@mff.cuni.cz)

J.-A. Sauvaud, A. Fedorov, H. Stenuit, Centre d'Etude Spatiale des Rayonnements, 9 Avenue du Colonel Roche, 31028 Toulouse Cedex 4, France.

S. A. Fuselier, Lockheed Palo Alto Research Laboratory, Palo Alto, CA 94304, USA.
S. Savin, L. Zelenyi, Space Research Institute, Profsoyuznaya 84/32, 117997 Moscow, Russia.
J. Berchem, University of California, Institute Geophysics and Planetary Physics, 405 Slichter Ave, Los Angeles, CA 90095 USA.

(Received February 2, 2003.)

Figure Captions:

Figure 1
Observational probability of a particular IMF B_Z value (a), and declination of IMF from the ecliptic (b).

Figure 2
Locations of satellites in GSM co-ordinates.

Figure 3
Solar wind and IMF conditions during analyzed interval. From top to bottom: solar wind dynamic pressure; the IMF magnitude and B_X component; IMF B_Y and B_Z components; the magnetosheath magnetic field magnitude and B_X component; magnetosheath B_Y and B_Z; the plasma sheet magnetic field magnitude and B_X component; B_Y and B_Z components in the plasma sheet. The subscripts in names of panels denote the particular spacecraft. Note that the WIND data are shifted on estimated propagation time.

Figure 4
Geomagnetic indexes, AE and D_{ST} during the analyzed interval.

Figure 5
Field lines of the Tsyganenko 96 model (blue) and INTERBALL-1 trajektory (red). INTERBALL-1 moves dawnward and upward. The black circle denotes the magnetopause crossing. Thin short black abscissae show the measured magnetic field.

Figure 6
An overview of INTERBALL-1 measurements. From top to bottom: f_{VDP} - tailward ion flux; B - magnetic field magnitude; B_{gsm} - components of the magnetic field; f_{DOKpar} - flux of 51 keV (red) and 111 keV (blue) protons in the sunward direction; $f_{DOKperp}$ - the same fluxes measured perpendicularly to the s/c spin axis; E_{C30} and E_{C150} - ion energy spectrograms measured in sunward and tailward directions, respectively; E_{e0} - electron energy spectrogram. Vertical lines divide the encountered regions.

Figure 7
An overview of MAGION-4 observations. From top to bottom: f - tailward ion flux; B - magnetic field magnitude, B_{gsm} - components of the magnetic field; E_{i0}, E_{i90}, and E_{i180} - ion energy spectrograms measured in tailward, perpendicular, and sunward directions, respectively. Note that the spacecraft spins approximately around the Sun-Earth line with a period ~ 7 minutes.

Figure 8
Electron, H^+ and O^+ energy spectrograms in the auroral region as measured by INTERBALL-2. The corresponding pitch angles are shown below.

Figure 9
Electron (a) and ion (b) energy spectra as measured by INTERBALL-1 and 2 in the magnetosheath, outer cusp, and LLBL. See text for description.

Figure 10
Polar observations of H^+ and O^+ inside the auroral region.

Figure 11
Footprints of the orbit of analyzed satellites (for the northern hemisphere). Depicted time intervals are listed in Table 1. The squares mark the places where cleft plasma was observed. Note that INTERBALL-1 (red) and MAGION-4 (pink) observed the cusp-like plasma along the whole projected part of the orbit.

Figure 12
The same as Figure 11, for the southern hemisphere.

Figure 13
A 3-D sketch of the magnetic field geometry showing possible merging sites when IMF is dominated by the B_Y component.

Figure 14
Changes of plasma parameters during the magnetopause crossing as derived from CORALL ion energy spectra (INTERBALL-1). From top to bottom: the ion density, n; the magnetic field magnitude, B; ion bulk speed, v; Alfvén velocity, v_A calculated form measurements above.

Figure 15
2-D cuts of 3-D ion velocity distributions as measured in the outer cusp (a), in the reconnection layer (b), and in the magnetosehath (c). The magnetic field points in the $+Z$ direction, $+Y$ is the direction of the convection velocity.

Figure 16
Count rate and corresponding pitch angle measured in the outer cusp (a), reconnection layer (b), and magnetosheath proper (c). The proton energy rises from $\sim$ 23 keV in top panels through 51 keV in middle panels to 111 keV in botom panels.

Figure 17
A schematics illustrating the flows of energetic protons. Line A corresponds to the magnetosheath proper, line B represents the magnetosheath field line near the magnetopause and C is the line inside the reconnection layer. Whereas lines A and B are supplied from the bow shock, the source of the particles observed on the line C is the cusp.

Figure 18
A 3-D sketch of the magnetic field lines formed by reconnection duskward of the northern cusp. The reconnected field line is depicted in green, directions of the motion of the kinks created by reconnection are shown by arrows. See text for a detailed description.

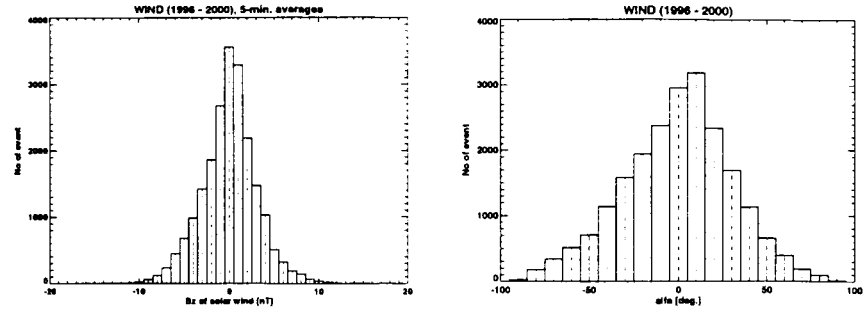

Figure 1: Observational probability of a particular IMF B_Z value (a), and declination of IMF from the ecliptic (b).

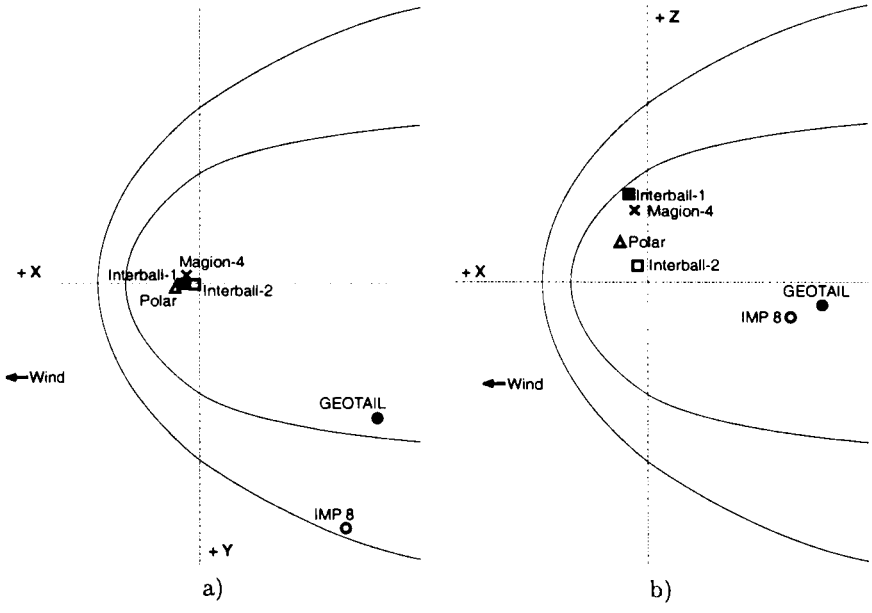

Figure 2: Locations of satellites in GSM co-ordinates.

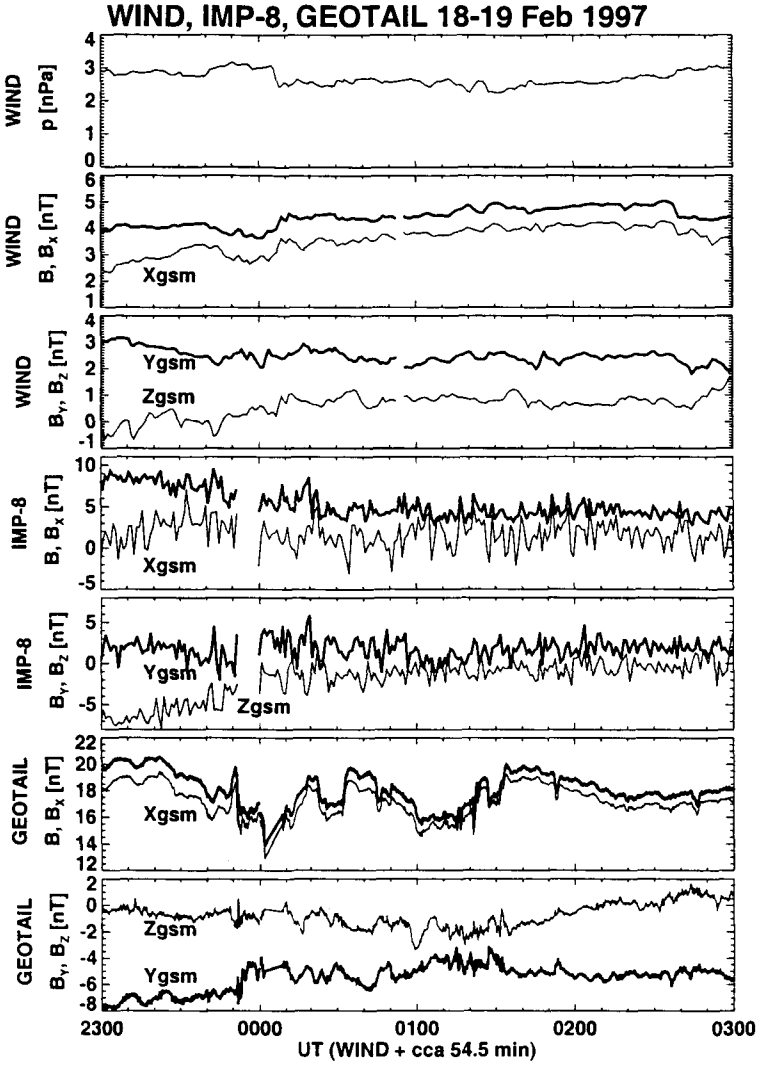

Figure 3: Solar wind and IMF conditions during analyzed interval. From top to bottom: solar wind dynamic pressure; the IMF magnitude and B_X component; IMF B_Y and B_Z components; the magnetosheath magnetic field magnitude and B_X component; magnetosheath B_Y and B_Z; the plasma sheet magnetic field magnitude and B_X component; B_Y and B_Z components in the plasma sheet. The subscripts in names of panels denote the particular spacecraft. Note that the WIND data are shifted on estimated propagation time.

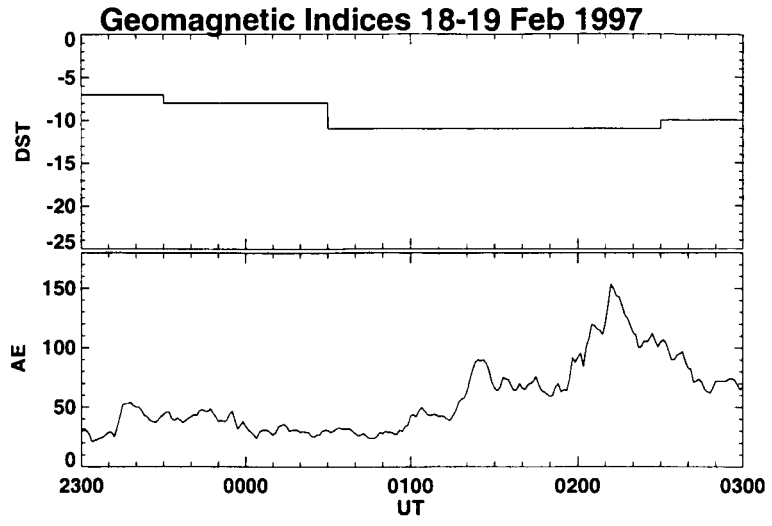

Figure 4: Geomagnetic indexes, AE and D_{ST} during the analyzed interval.

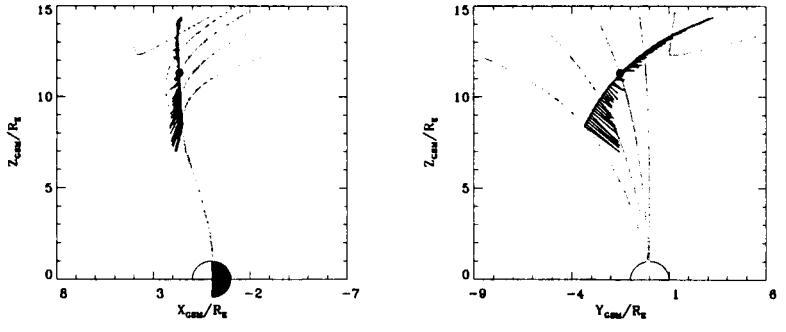

Figure 5: Field lines of the Tsyganenko 96 model (blue) and INTERBALL-1 trajektory (red). INTERBALL-1 moves dawnward and upward. The black circle denotes the magnetopause crossing. Thin short black abscissae show the measured magnetic field.

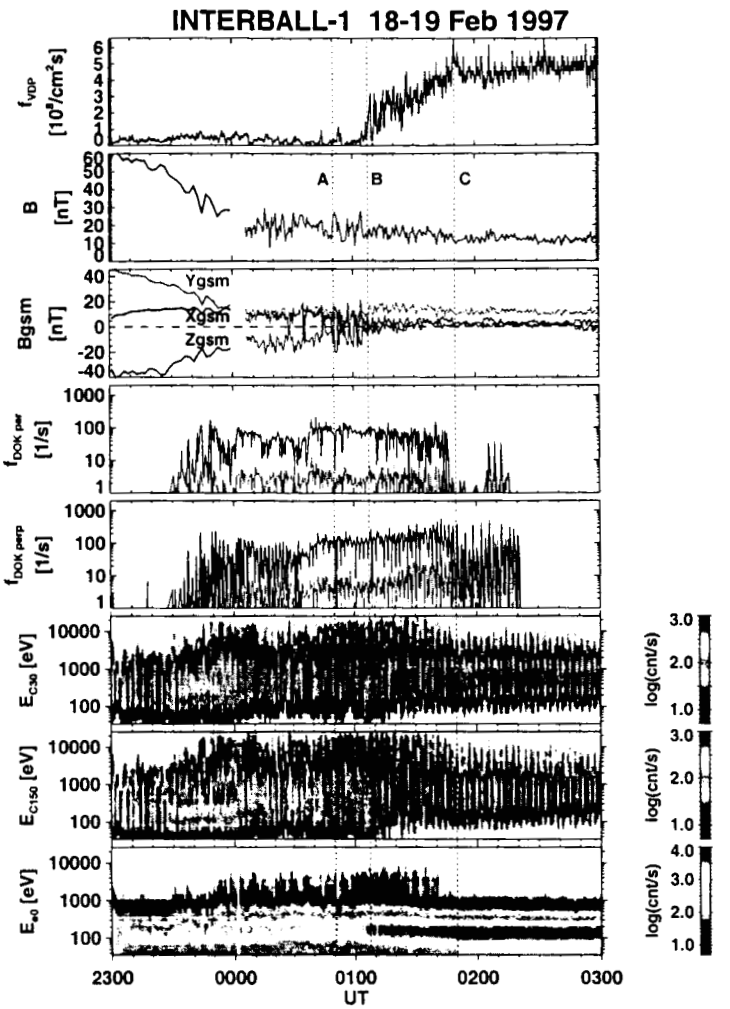

Figure 6: An overview of INTERBALL-1 measurements. From top to bottom: f_{VDP} - tailward ion flux; B - magnetic field magnitude; B_{gsm} - components of the magnetic field; f_{DOKpar} - flux of 51 keV (red) and 111 keV (blue) protons in the sunward direction; $f_{DOKperp}$ - the same fluxes measured perpendicularly to the s/c spin axis; E_{C30} and E_{C150} - ion energy spectrograms measured in sunward and tailward directions, respectively; E_{e0} - electron energy spectrogram. Vertical lines divide the encountered regions.

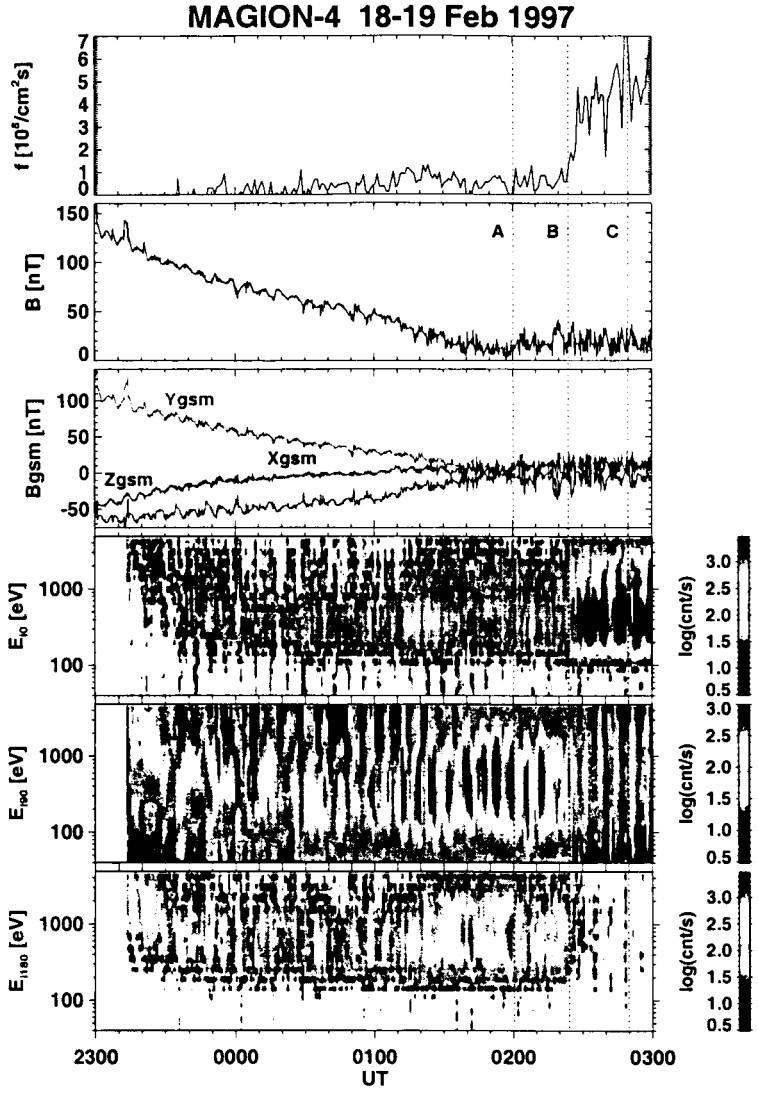

Figure 7: An overview of MAGION-4 observations. From top to bottom: f - tailward ion flux; B - magnetic field magnitude, B_{gsm} - components of the magnetic field; E_{i0}, E_{i90}, and E_{i180} - ion energy spectrograms measured in tailward, perpendicular, and sunward directions, respectively. Note that the spacecraft spins approximately around the Sun-Earth line with a period $sim7$ minutes.

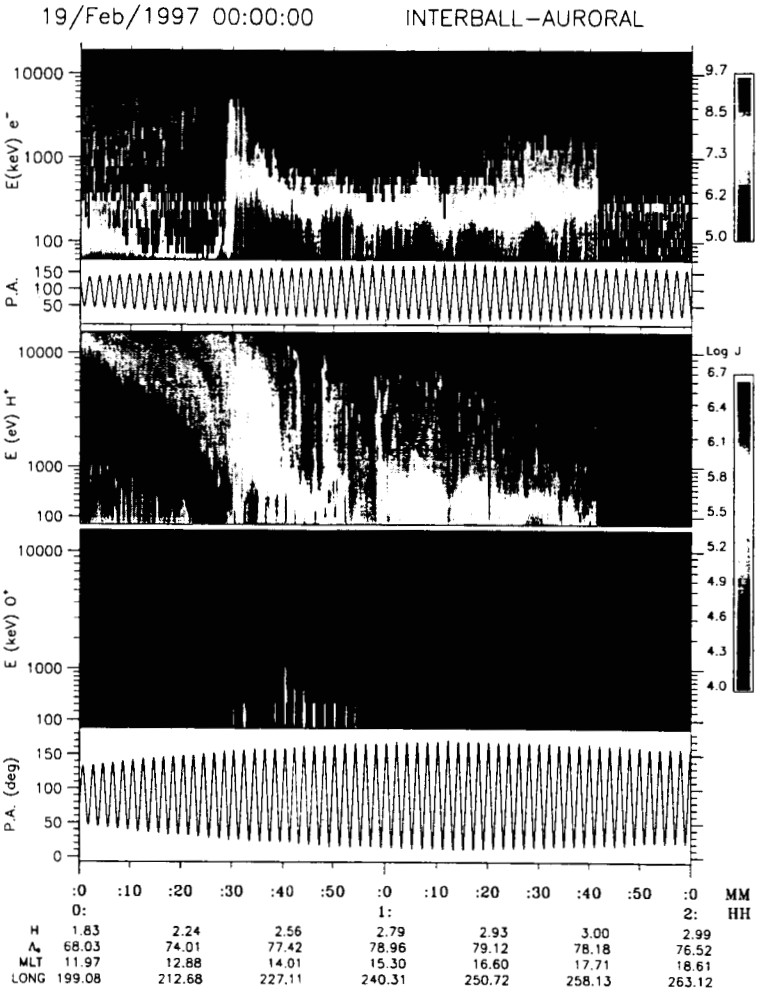

Figure 8: Electron, H^+ and O^+ energy spectrograms in the auroral region as measured by INTERBALL-2. The corresponding pitch angles are shown below.

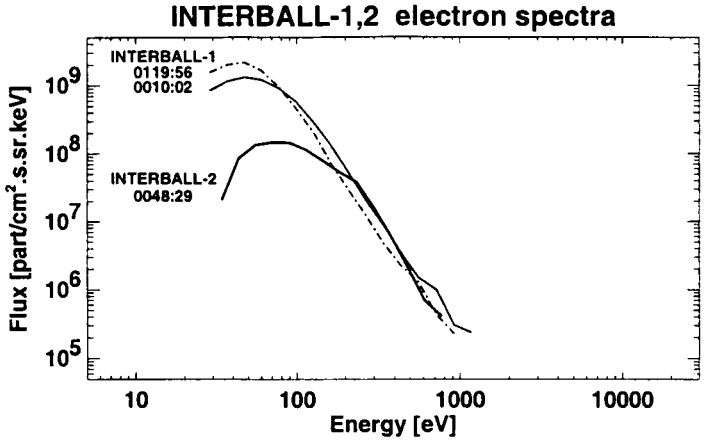

a)

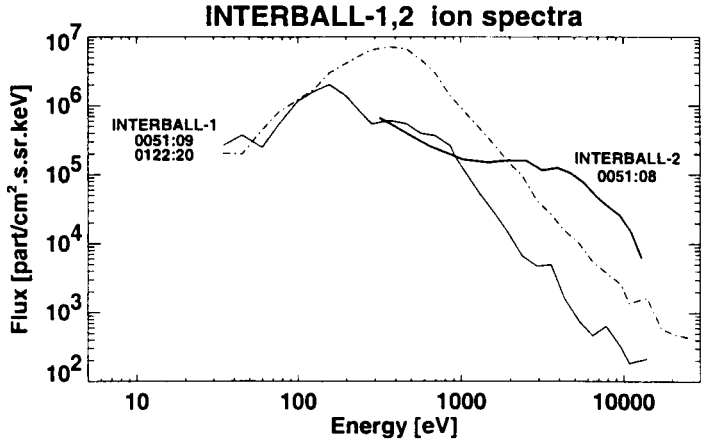

b)

Figure 9: Electron (a) and ion (b) energy spectra as measured by INTERBALL-1 and 2 in the magnetosheath, outer cusp, and LLBL. See text for description.

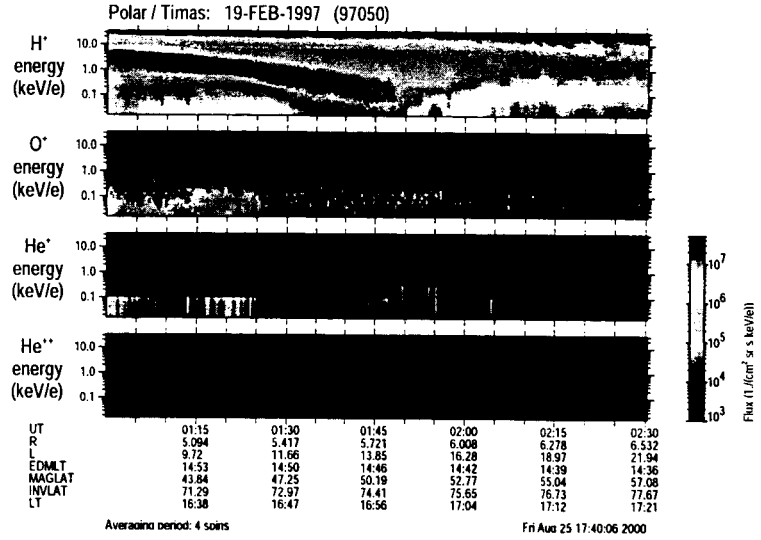

a)

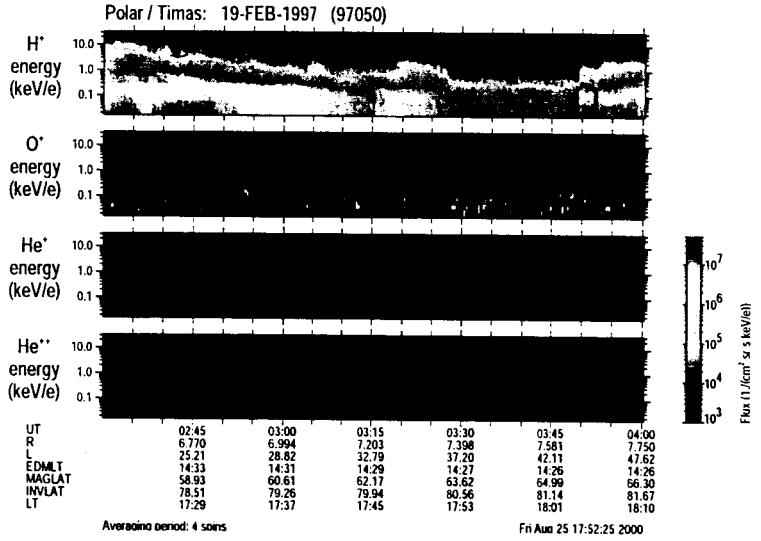

b)

Figure 10: Polar observations of H^+ and O^+ inside the auroral region.

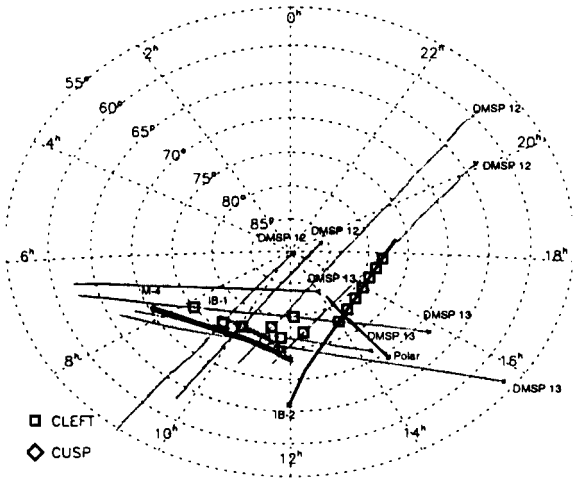

Figure 11: Footprints of the orbit of analyzed satellites (for the northern hemisphere). Depicted time intervals are listed in Table 1. The squares mark the places where cleft plasma was observed. Note that INTERBALL-1 (red) and MAGION-4 (pink) observed the cusp-like plasma along the whole projected part of the orbit.

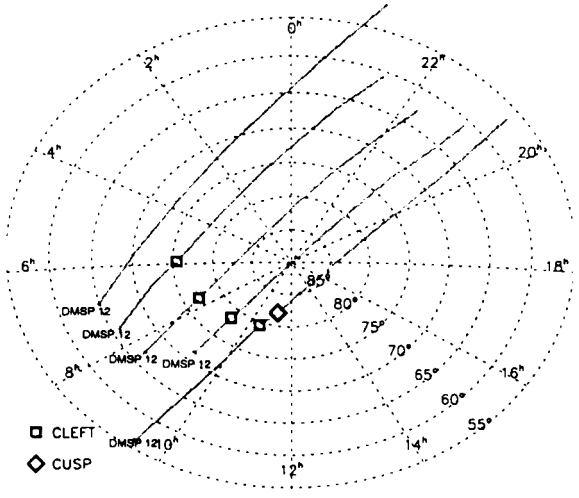

Figure 12: The same as the figure 11, for the southern hemisphere.

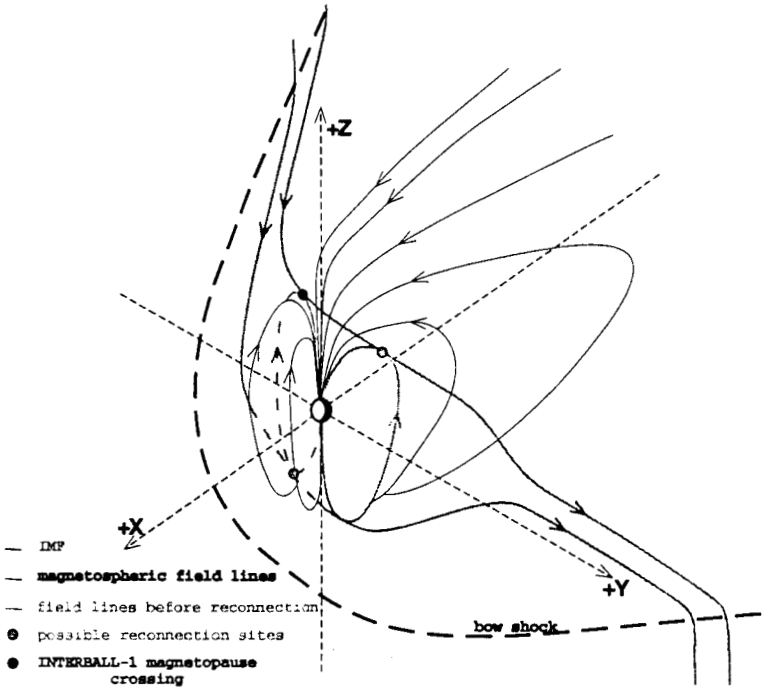

Figure 13: A 3-D sketch of the magnetic field geometry showing possible merging sites when IMF is dominated by the B_Y component.

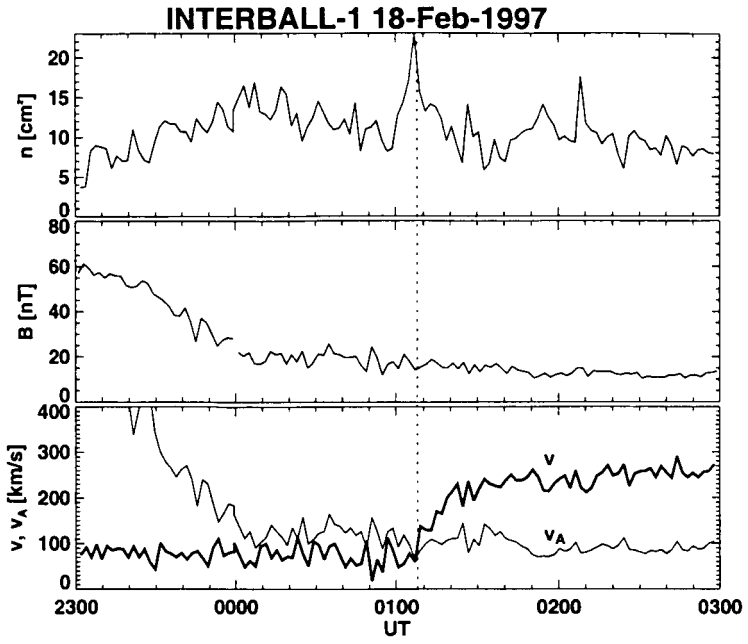

Figure 14: Changes of plasma parameters during the magnetopause crossing as derived from CORALL ion energy spectra (INTERBALL-1). From top to bottom: the ion density, n; the magnetic field magnitude, B; ion bulk speed, v; Alfvén velocity, v_A calculated form measurements above.

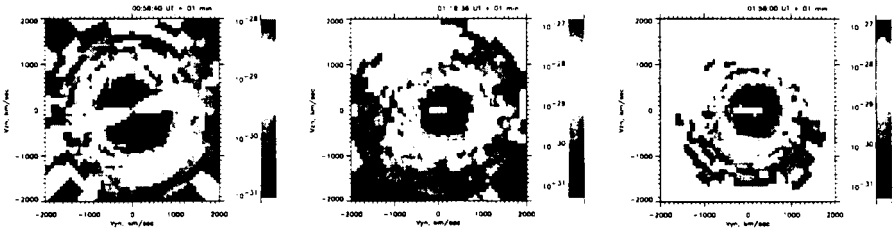

Figure 15: 2-D cuts of 3-D ion velocity distributions as measured in the outer cusp (a), in the reconnection layer (b), and in the magnetosehath (c). The magnetic field points in the $+Z$ direction, $+Y$ is the direction of the convection velocity.

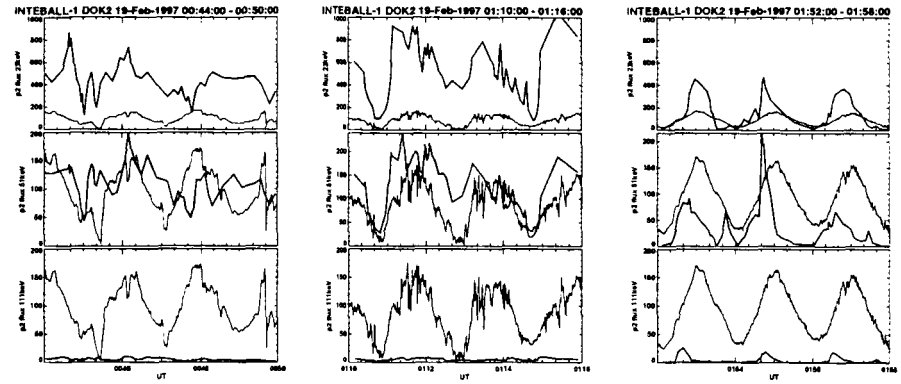

Figure 16: Count rate and corresponding pitch angle measured in the outer cusp (a), reconnection layer (b), and magnetosheath proper (c). The proton energy rises from *sim*23 keV in top panels through 51 keV in middle panels to 111 keV in botom panels.

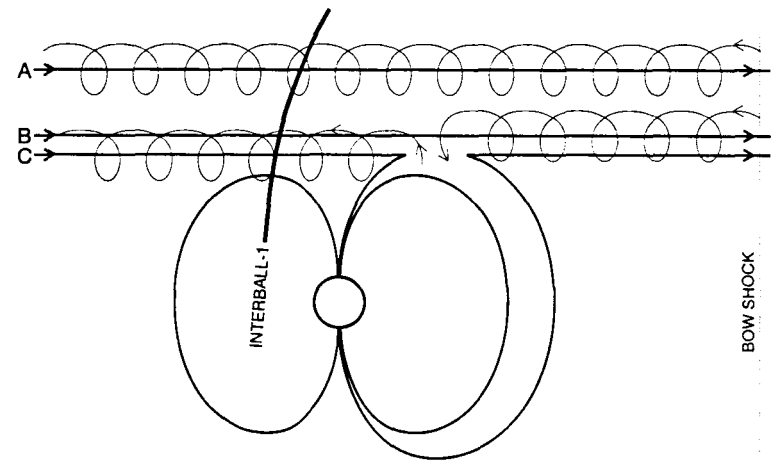

Figure 17: A schematics illustrating the flows of energetic protons. Line A corresponds to the magnetosheath proper, line B represents the magnetosheath field line near the magnetopause and C is the line inside the reconnection layer. Whereas lines A and B are supplied from the bow shock, the source of the particles observed on the line C is the cusp.

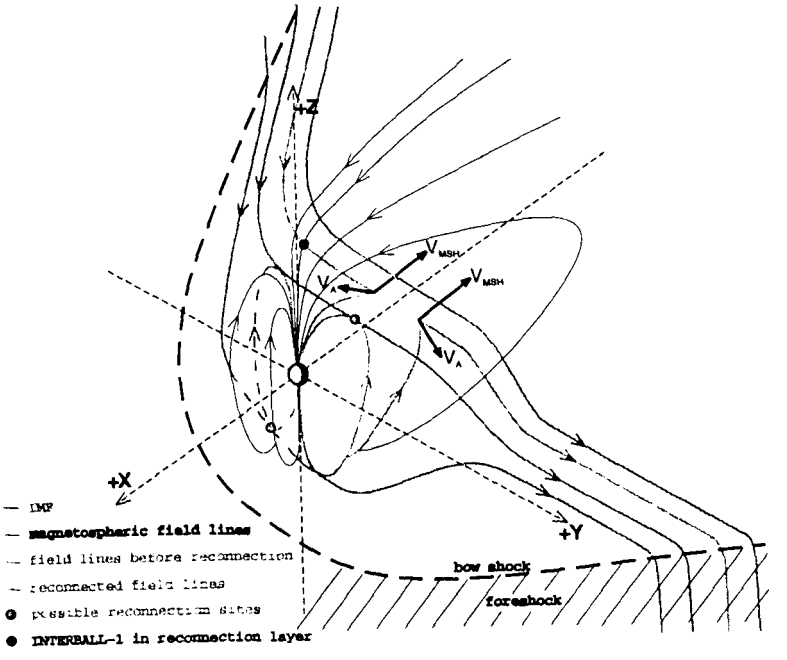

Figure 18: A 3-D sketch of the magnetic field lines formed by reconnection duskward of the northern cusp. The reconnected field line is depicted in green, directions of the motion of the kinks created by reconnection are shown by arrows. See text for a detailed description.